Sintering of two-dimensional nanoclusters in metal(100) homoepitaxial systems: Deviations from predictions of Mullins continuum theory

Da-Jiang Liu[1] and J. W. Evans[1,2]
[1]*Ames Laboratory–USDOE, Iowa State University, Ames, Iowa 50011*
[2]*Department of Mathematics, Iowa State University, Ames Iowa 50011*
(Received 23 October 2001; revised manuscript received 18 January 2002; published 8 October 2002)

We present a comparison of the predictions of atomistic and continuum models for the sintering of pairs of near-square two-dimensional nanoclusters adsorbed on the (100) surface in fcc metal homoepitaxial systems. Mass transport underlying these processes is dominated by periphery diffusion (PD) of adatoms along the edge of the clusters. A Mullins-type continuum model for cluster evolution incorporates anisotropy in the step edge stiffness (reflecting the energetics and adsorption site lattice structure in the atomistic model), and can also account for anisotropy in the step edge mobility (reflecting details of the kinetics). In such continuum treatments, the characteristic time τ_{eq} for relaxation of clusters with linear size of order L satisfies $\tau_{eq} \sim L^4$. Deviations may generally be expected for small sizes L or low temperatures T. However, for the relaxation of *dumbbell-shaped clusters* (formed by corner-to-corner coalescence of square clusters), atomistic simulations for PD with no kink rounding barrier ($\delta=0$) reveal that $\tau_{eq} \sim L^4$ always applies. In contrast, atomistic simulations with a large kink rounding barrier ($\delta>0$) reveal distinct scaling with $\tau_{eq} \sim L^3$, for low T or small L, thus providing an effective way to test for $\delta>0$. For the relaxation of *faceted rectangular clusters* (formed by side-to-side coalescence of square clusters), atomistic simulations for PD with $\delta=0$ reveal that $\tau_{eq} \sim L^2$, for low T or small L. This is consistent with a recent proposal by Combe and Larralde. For large $\delta>0$, τ_{eq} has an even weaker dependence on L. We elucidate scaling behavior and the effective activation barrier for relaxation in terms of the individual atomistic PD processes and their barriers.

DOI: 10.1103/PhysRevB.66.165407 PACS number(s): 68.35.Fx, 68.35.Bs, 68.35.Md

I. INTRODUCTION

Metal(100) homoepitaxial systems allow the possibility to explore two-dimensional (2D) analogs of sintering processes,[1,2] traditionally studied in 3D systems.[3] By deposition of up to 0.3–0.4 monolayers (ML's) of atoms on a perfect terrace, one can create distributions of isolated 2D adatom islands or clusters, each of which has a near-square equilibrated shape. Nearby pairs of islands can collide or coalesce either by growth during deposition, or alternatively by post-deposition diffusion. Thereafter, one can monitor the post-deposition restructuring of such pairs to form a single larger near-square island (i.e., sintering). Based on previous experimental studies of these systems,[1,2,4,5] we believe that the mass transport underlying sintering is dominated by periphery diffusion (PD) of adatoms along island edges (but see Ref. 6). Then, a 2D version of a Mullins-type continuum theory for shape evolution via PD (Ref. 7) makes specific predictions for the time evolution, and its scaling with linear feature size L (which is always given below in units of the lattice constant). For example, the characteristic time τ_{eq} for restructuring or equilibration via PD should satisfy $\tau_{eq} \sim L^n$, with scaling exponent $n=4$ (in two dimensions).[8] How well are these predictions satisfied for nanoscale 2D metal homoepitaxial islands under typical experimental conditions?

Extensive experimental data and atomistic simulation analyses are available for the size scaling of these 2D sintering and restructuring processes for the Ag/Ag(100) system at 300 K.[1] The data suggest some deviation from the scaling predictions of continuum theory for PD, with perhaps $\tau_{eq} \sim L^3$, i.e., with scaling exponent $n=3$ (although experimental uncertainty is substantial). Observations of analogous PD-dominated sintering phenomena are also available for Cu/Cu(100) at 300 K.[2] Indeed, the experimental observations for sintering of 2D adatom islands in these two systems primarily motivates the detailed theoretical modeling and analysis in this paper.

However, it is appropriate to note that several aspects of our analysis will have more general applicability than just to adatom island sintering in metal(100) homoepitaxial systems. One can examine the analogous processes for advacancy islands, which can be created either by sputtering, or by deposition of just below 1 ML of atoms. Limited analysis of the sintering of such near square advacancy islands at 300 K is in fact available for Ag/Ag(100) (Ref. 1) and for Ni/Ni(100)[9] (although strain effects seem significant in the latter system). Also, similar phenomena have been observed for metal(111) homoepitaxial systems, where equilibrium island shapes are near-hexagonal rather than near-square. For both Ag/Ag(111)[10] and Cu/Cu(111),[11] it is believed that again PD dominates. For the sintering of advacancy island pairs in the Ag/Ag(111) system at 300 K, deviations from the predictions of continuum theory for PD have been suggested (although again uncertainty in experimental data precludes a definitive analysis).[10]

Comparison of behavior of atomistic models for interface evolution with appropriate continuum theories is a well-established area in statistical physics. There are extensive studies of evolution of surfaces in three dimensions by surface diffusion (or other processes), most of which focus on flattening (or smoothening) of grooves on surfaces. In general, continuum theories which incorporate appropriate system-dependent parameters (surface or step edge stiffness

and mobility) should recover the behavior of the atomistic model for temperatures above the roughening transition (in three dimensions), and for sufficiently large characteristic length scales. Continuum modeling below the roughening transition is still a challenging problem. There are also studies of the corresponding problem in two dimensions using 1+1D solid-on-solid (SOS) models, which show good agreement with Mullins' continuum theory for capillary waves in the regime of small slopes[12] By incorporating anisotropy in stiffness and mobility one can extend the predictive capabilities of the continuum theory even to the regime of steep slopes. Notable is a study of Krug *et al.*[13] which shares much of the same methodology as the continuum modeling that we will use later.

Relaxation of 2D clusters introduces two complications to a continuum description relative to the above flattening problem. First the complicated geometry prevents linearizing the dynamical equation around the long-time asymptotic solution. The resulting nonlinearity can create singularities (specifically, breaking up or pinch off of clusters) even though the dynamical equation is everywhere continuous.[5] Second, incorporation of anisotropy in stiffness is essential to achieve the correct equilibrium shape. Perhaps due to these difficulties, previous atomistic simulations for the 2D sintering processes of interest here[10,11,14] have not been compared quantitatively with the associated continuum models incorporating appropriate anisotropies.

In general, one expects a breakdown of continuum description for sufficiently small island sizes, and likely also for sufficiently low temperatures (T) where islands are highly faceted. Indeed, recent theoretical studies revealed and analyzed such behavior, but only for a special case of perfectly *faceted* clusters with simple nonequilibrium *convex* shapes, and for a special prescription of PD dynamics *without* any corner or kink rounding barrier (see below).[14,15] For these convex faceted geometries at low T, the key step in shape relaxation is nucleation of a new edge, and analysis of this process indicates that $\tau_{eq} \sim L^2$, i.e., a scaling exponent of $n=2$. We also mention here an earlier somewhat similar analysis of cluster shape relaxation in Ref. 16. As an aside, we note that similar issues and concepts have also arisen in consideration of the related problem of the PD-mediated surface diffusion for large 2D clusters; see Appendix A.

A central goal of this paper is to provide a more comprehensive characterization of the various regimes or ways in which the continuum treatment can fail to describe behavior of atomistic models for cluster evolution via PD. Conversely, we are also interested in elucidating regimes where the continuum model is unexpectedly effective, e.g., despite small feature size. Success or failure should depend on both energetic and kinetic parameters of the atomistic model, as well as on feature morphology or shape. Thus we compare in detail predictions of the atomistic and continuum models developed in Sec. II for different parameter choices and shapes of the relaxing clusters. We analyze the relaxation of dumbbell-shaped clusters (formed by corner-to-corner coalescence of square clusters) in Sec. III A, and the relaxation of faceted rectangular clusters (formed by side-to-side coalescence) in Sec. III B. In the absence of a kink rounding barrier for PD, we find deviations from continuum scaling for faceted clusters, consistent with previous work, but no such deviations for dumbbell-shaped clusters. An additional key component of this paper is analysis of the effect on relaxation of introducing a large kink rounding barrier for PD. We find distinct scaling behavior from the case of no barrier for both the above geometries. Furthermore, we argue that a particular effective way to assess the existence and magnitude of a kink rounding barrier is by analysis of the relaxation of dumbbell-shaped clusters. In Sec. IV, we elucidate observed scaling behavior, as well as the effective activation barriers controlling the overall relaxation processes, in terms of the individual atomistic PD processes and their barriers. Concluding remarks are provided in Sec. V.

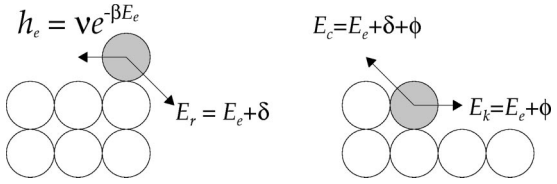

FIG. 1. Schematics of the atomistic PD model showing the four atomic hopping processes (for the shaded atom): edge diffusion at rate h_e and activation barrier E_e, corner rounding with barrier E_r, kink escape with barrier E_k, and core breakup with barrier E_c.

II. ATOMISTIC PD MODEL AND ITS CONTINUUM FORMULATION

A. Atomistic PD model

Similar to previous studies,[1,16] we develop a simplified but realistic lattice-gas model for 2D nanocluster evolution via PD in metal(100) homoepitaxial systems. In this model, we consider clusters of adatoms connected by nearest-neighbor (NN) bonds on a square lattice of adsorption sites, for which periphery atoms can hop according to certain rules described in detail below. To inhibit the alternative detachment-reattachment pathway for mass transport (as justified below), we exclude hops which lead to periphery atoms detaching and becoming isolated, i.e., having no NN atom in the cluster. Due to this constraint, we must allow periphery atoms to make *both* NN and second NN (2NN) hops in order for such dynamics to incorporate unrestricted PD. More specifically, 2NN hops are necessary to allow rounding of kinks and corners (which in reality occurs as a ''difficult'' NN hop to a site with one 2NN but no NN cluster atoms, followed quickly by an ''easy'' NN hop back to a site with a NN cluster atom). Specific hopping rates reflect detailed-balance constraints consistent with assumed NN pairwise attractive interactions of strength ϕ.

In Fig. 1, we identify the most important elementary hopping processes in our model. Key processes involving NN hops are: (i) rapid ''edge diffusion'' along straight close-packed [110] step edges with ''low'' barrier E_e; (ii) ''kink escape'' along straight [110] step edges with barrier $E_k = E_e + \phi$. Key processes involving 2NN hops are: (iii) ''corner rounding'' with barrier $E_r = E_e + \delta$; (iv) ''core breakup'' with barrier $E_c = E_e + \delta + \phi$. In (iii), δ represents an additional

barrier for corner or kink rounding relative to edge diffusion; δ is sometimes referred to as the ''kink Ehrlich-Schwoebel barrier.''[17] A consistent choice of rates for NN hopping (h^{NN}) and 2NN hopping (h^{2NN}) has the form

$$h^{\mathrm{NN}} = \nu \exp\{-[E_e + (n_i - 1)\phi]/(k_B T)\}, \tag{1}$$

and

$$h^{\mathrm{2NN}} = \nu \exp\{-[E_e + \delta + (n_i - 1)\phi]/(k_B T)\}, \tag{2}$$

where n_i is the initial number of NN cluster atoms before hopping, and the final number of NN cluster atoms satisfies $n_f \geqslant 1$. In Eqs. (1) and (2), ν is an attempt frequency for hopping which, for simplicity, is assumed to have a common value for both NN and 2NN hops. These formulas also provide rates for other less significant processes such as extraction of an atom from a straight [110] step edge via a 2NN hop with barrier $E_e + \delta + 2\phi$. If h_i (with $i = e,k,r,c$, etc.) denote the rates for these various hopping processes, then detailed balance imposes the constraints that $h_k/h_e = h_c/h_r = \exp[-\phi/(k_B T)] \equiv \rho (\ll 1$, typically). Below, it is convenient to introduce the corresponding characteristic times, $\tau_i = 1/h_i$.

For restructuring of nonfaceted features, the effective activation barrier in our PD model, $E_{\mathrm{act}}(\mathrm{PD})$, often corresponds to the barrier for the ''slow'' core breakup process, i.e., $E_{\mathrm{act}}(\mathrm{PD}) = E_c = E_e + \delta + \phi$ (but see below).[1,18] This $E_{\mathrm{act}}(\mathrm{PD})$ should be compared with the effective barrier for detachment and reattachment of periphery adatoms mediated by terrace diffusion (TDA) of $E_{\mathrm{act}}(\mathrm{TDA}) = E_d + 2\phi$, or with that for terrace diffusion of vacancies (TDV) through the interior of the cluster of $E_{\mathrm{act}}(\mathrm{TDV}) = E_v + 2\phi$.[18] Here, $E_d (E_v)$ denotes the activation barrier for terrace diffusion of isolated adatoms (isolated advacancies).

For metal(100) homoepitaxial systems, semiempirical studies of energetics suggest that $\delta \ll \phi$.[19] Also, a combination of semiempirical, *ab initio*, and experimental data shows that E_e is well below both E_d and E_v. For Ag/Ag(100), one has $E_d = 0.40$–0.45 eV,[20,21] $E_v/E_d \approx 0.95$, and $E_e = 0.25$ eV.[21] For Cu/Cu(100), one has $E_d = 0.48$–0.52 eV,[22,23] $E_v = 0.42$ eV,[23] $E_e/E_d \approx 0.5$. Ratios are semiempirical estimates.[19] Thus PD has a *substantial energetic advantage* over both TDA and TDV, explaining its dominance in these systems.

We close with a few additional comments on our model. First, the above choice of rates implies that the barrier for diffusion along perfect open [100] step edges E_e^* equals the core breakup barrier E_c. In general, E_e^* could be different from (and most likely lower than) E_c. Semiempirical EAM calculations for the Ag/Ag(100) system yield $E_e^* = 0.73$ eV, whereas $E_e = 0.28$ eV and $\phi = 0.28$ eV, so $E_c = 0.84$ eV.[24] Likely, behavior with these parameters is similar to that for our choice with $E_e^* = E_c$. Second, our model does not incorporate exchange diffusion processes. However, it is quite plausible that the easiest pathway for corner rounding is via exchange, at least at single atom high kinks. In this case, estimates for δ obtained from comparing our model with experiment might be interpreted as corresponding to exchange rather than conventional corner rounding.[18] Finally, we note that disconnected cluster configurations, as well as advacancies, can be created indirectly in our model, but these events are rare and have negligible effect. See Appendix B for further details and discussion.

B. Continuum formulation

The continuum formulation of the shape evolution of 2D clusters via PD has been developed in recent works.[14,5] In the continuum model, the morphology of a 2D cluster is described by a closed plane curve, represented parametrically as $\mathbf{r}(s) = (x(s), y(s))$. Its evolution is determined by its normal velocity, which can be determined using local mass conservation. For PD, it is given by

$$v_n(s,t) = \Omega \nabla_\tau J_{\mathrm{PD}}(s,t), \tag{3}$$

where J_{PD} is the atomic flux along the perimeter, and $\nabla_\tau = (x_s^2 + y_s^2)^{-1/2} \partial/\partial s$ is the derivative with respect to the arc length along the perimeter, and Ω is the area of the unit cell. From linear response theory, one has

$$J_{\mathrm{PD}} = -\frac{\sigma_{\mathrm{PD}}}{k_B T} \nabla_\tau \mu, \tag{4}$$

where μ is the chemical potential of step edge atoms which measures the energy cost for adding atoms to the step, and σ_{PD} is a coefficient measuring the mobility of step edge atoms.

In the continuum model, σ_{PD} and μ depend only on the local configuration. Specifically, one can write

$$\mu = \Omega \tilde{\beta}(\theta) \kappa(s), \tag{5}$$

where $\theta = \theta(s)$ is the local azimuthal angle of the step edge, and κ is the local curvature. $\tilde{\beta}$ is the stiffness of the step edge, which is related to step edge energy $\beta(\theta)$ through $\tilde{\beta} = \beta(\theta) + \beta''(\theta)$. Similarly, we assume σ_{PD} is a function of the local azimuthal angle, i.e., $\sigma_{\mathrm{PD}} = \sigma_{\mathrm{PD}}[\theta(s)]$. The detailed forms of $\beta(\theta)$ and $\sigma_{\mathrm{PD}}(\theta)$ depend on the microscopic energetic and dynamical properties of the step edge. In our formalism, J_{PD} has the dimensions of (atoms)/s, ∇_τ of Å^{-1}, Ω of Å^2, v_n and σ_{PD} of Å/s, μ of eV, and β (or $\tilde{\beta}$) of eV/Å.

One important simplification is to assume both σ_{PD} and β to be constant, which leads to the *isotropic continuum model*.[5,14] Here we focus on the anisotropies of these two quantities.

By assuming only NN interactions in the microscopic model of Sec. II A, the corresponding Ising model step edge free energy $\beta(\theta)$ can be solved analytically for the square lattice as[25]

$$\beta(\theta) = k_B T[|\cos\theta| \sinh^{-1}(\alpha|\cos\theta|) + |\sin\theta| \sinh^{-1}(\alpha|\sin\theta|)], \tag{6}$$

where

$$\alpha = \frac{2}{b}\left[\frac{1 - b^2}{1 + (\sin^2 2\theta + b^2 \cos^2 2\theta)^{1/2}}\right]^{1/2}, \tag{7}$$

and

$$b = \frac{2\sinh[\phi/(2k_BT)]}{\cosh^2[\phi/(2k_BT)]}. \quad (8)$$

Solutions are also available for triangular and honeycomb lattices.[26]

The mobility coefficient $\sigma_{\rm PD}$ depends on the dynamics of the underlying microscopic model. We relegate the details of this analysis to Appendix C and summarize here only its basic properties.

As with $\beta(\theta)$, $\sigma_{\rm PD}$ exhibits fourfold symmetry associated with the underlying square lattice (with lattice constant a). If $\delta=0$, we have that (cf. Ref. 13)

$$\sigma_{\rm PD}(\theta) \approx a\nu \exp[-(E_e+\phi)/(k_BT)] \quad (9)$$

is approximately isotropic. For $\delta>0$, $\sigma_{\rm PD}$ exhibits its maxima at the four close-packed directions and decreases rapidly as θ deviates from these directions. Around the open [100] step edge directions it is relatively flat. It has the following form:

$$\sigma_{\rm PD}(\pi/4) \approx f(\delta) a\nu \exp[-(E_e+\delta+\phi)/(k_BT)], \quad (10)$$

where $f(\delta)$ is a prefactor which increases from 1 to about 3 when δ increases from 0 to ϕ, and remains approximately constant as δ increases further.

To solve the continuum model numerically, we use the so-called Lagrangian approach[27] coupled with the ''method of lines.''[28] First we discretize the continuous curve and covert the partial differential equation (PDE) (3)–(5) to a set of ordinary differential equations (ODE's). Then, we integrate numerically the ODE's using Gear's backward differentiation formulas (BDF) method since the resulting ODE's are stiff equations. For simplicity and to minimize discretization errors, we choose the grid points to be evenly spaced so that the arc lengths between consecutive points are the same. Subsequent evolution, however, will destroy this spatial uniformity. We thus periodically adjust the grid points by spline fitting so that they are always near evenly spaced. Typically we use 128 grid points on each curve and readjust the grid points 100 times during the relaxation process. In general, readjustment of grid points can introduce unwanted distortion to the solution of the PDE. We test empirically the numerical accuracies of the solutions by checking that they display weak sensitivity to both the number of grid points and the frequency of grid point readjustment.

III. RESULTS FOR RELAXATION DYNAMICS DURING SINTERING

A. Dumbbell-shaped clusters (corner-to-corner coalescence)

For simplicity, we consider an initial configuration where two equal sized near-square clusters are touching corner to corner. We monitor the subsequent evolution, focusing on growth of the neck between them during the sintering or restructuring process (which leads to a single larger near-square island). There are experimental examples of this scenario for the Ag/Ag(100) and Cu/Cu(100) systems.[1,2] In atomistic simulations with perfectly square $L\times L$ initial clusters having diagonally adjacent corner atoms, the clusters actually tend to separate or pinch off rather than sinter for sufficiently large linear sizes. This is avoided in our atomistic simulations by shifting the two outer corner atoms to the neck and thus thickening the initial neck (the total number of atoms remaining at $2L^2$). In the continuum analysis, we simply preclude pinch off. One could certainly avoid pinch off by starting with more complex initial conditions (e.g., touching clusters with equilibrated shapes mimicking experiment), but we believe that the basic behavior of neck growth would be unchanged.

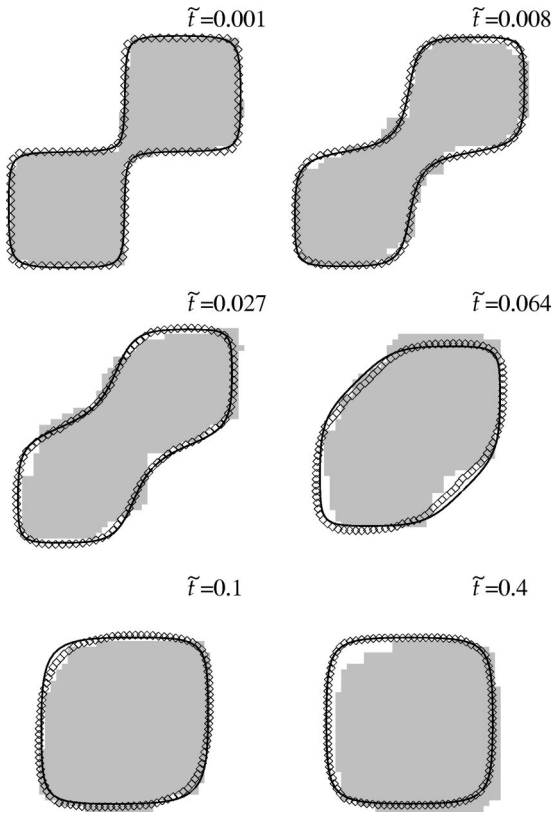

FIG. 2. Snapshots of the sintering process of two clusters joined by their corners. The solid line is the result of continuum model with constant $\sigma_{\rm PD}$ and the symbols are results (average of 100 MC runs) of the atomistic model with $L=20$. Other parameters are $\phi=0.235$ eV, $\delta=0$, and $T=300$ K. Configurations of a single MC run are overlayed.

1. Results without corner rounding barrier ($\delta=0$): conventional scaling

First we present the continuum model predictions. It is easy to see that for the continuum model, the sintering process obeys a size scaling relationship: if $\tilde{\mathbf{r}}(t)$ is the solution of the continuum equation with the initial value $\mathbf{r}(0)=\tilde{\mathbf{r}}_0$, then $\lambda\tilde{\mathbf{r}}(t/\lambda^4)$ is the solution with the initial value $\lambda\tilde{\mathbf{r}}_0$. One immediate consequence is that the equilibration time $\tau_{\rm eq}$ (defined, e.g., as the time for the neck to grow to some constant times L) scales exactly as L^4. In our numerical analysis, we use only an isotropic mobility coefficient, i.e., $\sigma_{\rm PD}(\theta)=\sigma_0$ is a constant. Figure 2 shows six snapshots of the reshaping process.

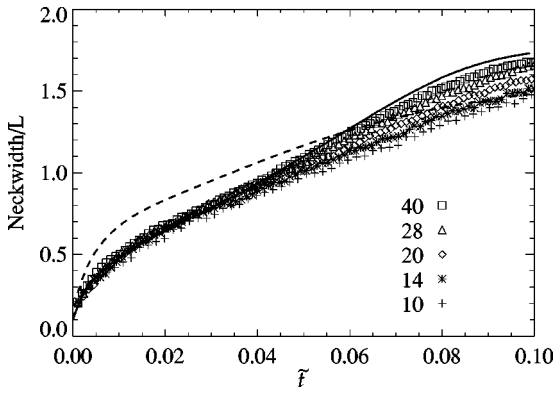

FIG. 3. Growth of the neckwidth measured along the diagonal, for $\phi=0.235$ eV and no extra corner rounding barrier at 300 K. Symbols are the average of 100 MC runs. The curves show results of the continuum model using (a) Ising step energy (solid) and (b) isotropic step energy (dashed).

We also perform kinetic Monte Carlo (KMC) simulations of the atomistic model to study the same sintering process. Details of the algorithm are given in Appendix B. First we observe that there are large fluctuations for small clusters. The sintering process can be quite different for different MC runs. Fluctuations become relatively smaller as the cluster size increases, in other words, the process becomes more deterministic. To compare results of the atomistic model with the continuum model, we average over configurations of different MC runs. Defining the average cluster boundaries as the points where the interpolated average site occupancies equal 1/2, we overplot the simulation results as symbols in Fig. 2. To compare the time scale in the continuum model with that in the KMC simulations, we use the formula $\sigma_{\rm PD}(\theta)=\sigma_0=ah_e e^{-\phi/(k_BT)}$ (see Sec. II B and Appendix C). In Fig. 2 we define $\tilde{t}=t\sigma_0\beta_{\rm av}(k_BTL^4)^{-1}$, where $\beta_{\rm av}=(2\pi)^{-1}\int_0^{2\pi}\beta(\theta)d\theta$. The agreement between the continuum prediction and KMC simulations is quite striking. The slight discrepancy in shapes apparent for $\tilde{t}=0.064$ effectively disappears for $L\gtrsim 50$. Also shown in Fig. 2 are configurations of a single MC simulation.

Perhaps a more striking result is how well the continuum model agrees with simulation results of even smaller L. Figure 3 shows the growth of the neckwidth for L ranging from 10 to 40, corresponding to about 3–12 nm on metal surfaces, from KMC simulations of the atomistic model with $\phi=0.235$ eV and $\delta=0$ at 300 K. The x axis is the sintering time rescaled as in Fig. 2, and the y axis is the neckwidth divided by L. Results are averaged over 100 KMC runs. Also plotted as a solid line is the result of the continuum model using the Ising $\beta(\theta)$ for NN interactions $\phi=0.235$ eV and a constant $\sigma_{\rm PD}$. Both the scaling and quantitative behavior of the KMC model agree quite well with the continuum model. However, we stress that for smaller clusters, results of each individual simulation (or experiment for that matter) can be quite different from the continuum model. The agreement is only apparent after averaging over many samples. Another observation from our simulations is that the L^4 scaling persist to very low temperatures (not shown), which is the regime when typically one needs to seriously question the validity of the continuum model.

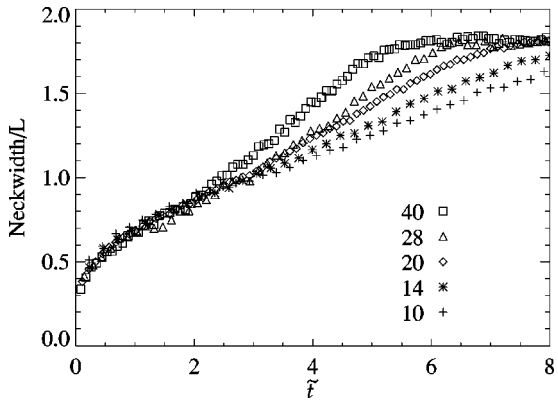

FIG. 4. Growth of the neck-width measure along the diagonal, for $\phi=0.235$ eV and extra corner rounding barrier $\delta=0.16$ eV at 300 K. Results for $L=10$–20 are averages of 100 MC runs, and results for $L=28$ and 40 are averages of 10 MC runs.

We also show for comparison the result of the *isotropic* continuum model in Fig. 3. The main difference is that here the growth rate of the neck width is strongly decreasing with time, while the results of the KMC model and the continuum model with Ising step energy show a near constant growth (except for the very beginning and the end of the sintering processes).

2. Results with large corner rounding barrier ($\delta>0$): Breakdown of scaling

Behavior is somewhat different when an large additional corner rounding barrier δ is present. Figure 4 plots neck growth from KMC simulations of the atomistic model with $\phi=0.235$ eV and $\delta=0.16$ eV at 300 K, again with time renormalized by L^4. Initially, the data collapse is quite good, reproducing the conventional L^4 scaling. However, after the neck width grows to about $0.8L$, this scaling starts to break down.

To measure the later stage growth rate, we fit the data in Fig. 4 for neck widths between $1.2L$ and $1.5L$ to a straight line as $a+R_Lt$. We then fit the growth rate R_L to L^{n-1}. (This type of analysis has also been employed in Ref. 1.) Results are shown in Fig. 5, along with results for $\delta=0$. Using data

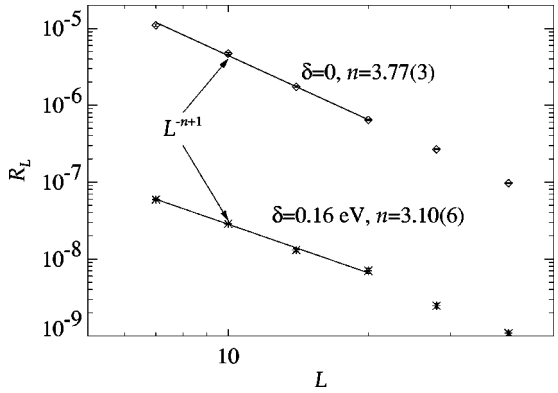

FIG. 5. MC results for the neck-width growth rate R_L, in unit of τ_e^{-1}. Key parameters are $\phi=0.235$ eV and $T=300$ K.

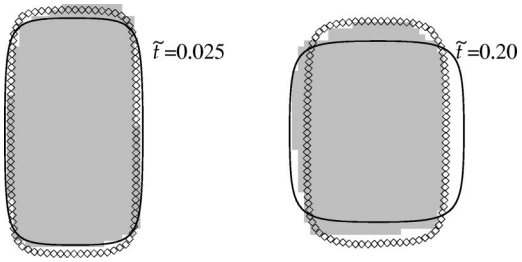

FIG. 6. Snapshots of the sintering process of two square clusters joined at one side. The solid line shows the continuum prediction. Symbols are the average of 100 MC runs of the atomistic model with ϕ=0.235 eV and δ=0 at 300 K, with $L=20$. Configurations of a single MC run are also overlayed.

for $L=7$ to $L=20$ we obtain $n=3.77(3)$ for the previous case with $\delta=0$, and $n=3.10(6)$ for $\delta=0.16$ eV. Note that the continuum model predicts $n=4$.

B. Faceted rectangular clusters (side-to-side coalescence)

Motivated by the predictions and analysis of Refs. 14 and 15 for relaxation of convex faceted clusters, we also consider the case of an initial rectangular configuration. Experimentally, such configurations are naturally created by side-to-side collision of clusters. Although typically clusters have different sizes, a near-rectangular configuration is quickly formed from the initial configuration of touching unequal sized squares. Then the metastable rectangular configuration slowly relaxes to the near-equilibrium square shape.[1]

1. Results without corner rounding barrier (δ=0)

Figure 6 shows two snapshots of the sintering process with $\delta=0$ for two clusters of size 20×20 joined at one side. Symbols are the average of cluster boundaries of 100 MC runs and solid line is the continuum model prediction. The energetics and temperature are the same as in Sec. III A. However, unlike the previous case, relaxation predicted by the continuum model is much too fast. Also shown are configurations of a single MC simulation.

Starting from a perfect rectangle of size $L\times2L$, we measure the aspect ratio by calculating the radii of gyration, r_x and r_y, as in Ref. 14. Figure 7 plots results of different system sizes using ϕ=0.235 eV and δ=0 at 300 K, with the prediction of the continuum model plotted as the solid line. In contrast to the results in Sec. III A and consistent with results in Refs. 14 and 15, there is a large discrepancy between the KMC results and the continuum model prediction for systems with $L<100$. Indeed, analysis of the decay of the aspect ratio is best described by an effective exponent $n=2.7$, rather than $n=4$ (see below).

2. Results with large corner rounding barrier ($\delta>0$)

As in Sec. III A, the presence of an extra corner rounding barrier δ shifts the size scaling exponent to an even lower number. Figure 8 shows the L dependence of the average relaxation time $\tau_{\rm eq}$ measured as the first time that the aspect ratio of the cluster reaches 1.5. Also shown for comparison are results of simulations and the prediction of the continuum

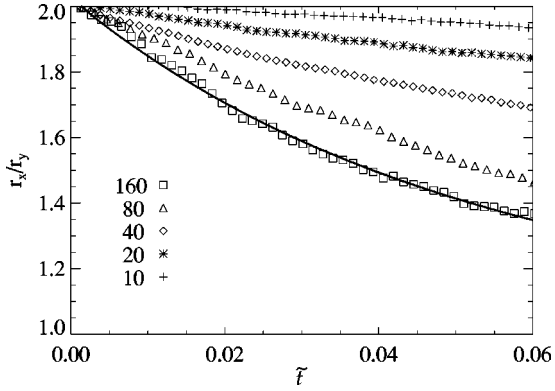

FIG. 7. Time dependence of the aspect ratio of rectangular islands of size $L\times2L$ for ϕ=0.235 eV and δ=0 at 300 K. The solid line is the prediction of the continuum model where r_x and r_y are the sizes of the cluster in the x and y directions, and the symbols are KMC simulation results where r_x and r_y are the gyration radii along the x and y directions.

model using $\delta=0$. Fitting the KMC simulations data for $L=5$ to 20 to a power law $\tau_{\rm eq}\sim L^n$ gives $n=2.7$ (for $\delta=0$) and $n=2.2$ (for $\delta=0.16$ eV) at 300 K. We can also see that for $L\gtrsim100$, results of the atomistic model with $\delta=0$ are closer to the continuum prediction. We expect that in both cases the scaling exponent will cross over to $n=4$ as L increases.

IV. DISCUSSION

Results in Sec. III reveal that the sintering of two nanoclusters can be characterized by a variety of size scaling exponents n, which for sufficiently small clusters deviate from the continuum prediction $n=4$. We emphasize that this deviation occurs even though mass transport is purely through periphery diffusion. As noted in Sec. I, such deviations have already been observed in both experiment and simulations. Furthermore, we will see that analytic theories[15,29] which have been developed to describe behavior

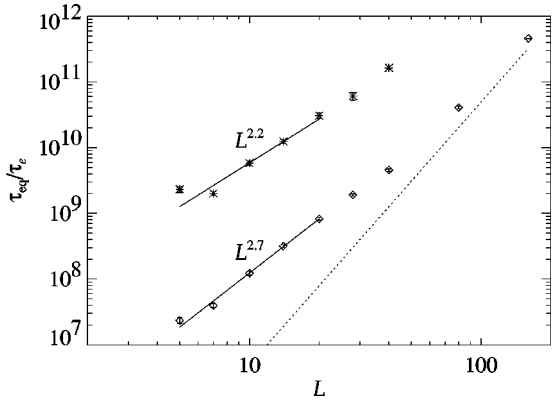

FIG. 8. Relaxation time $\tau_{\rm eq}$ (in unit of τ_e) measured as the first time that the aspect ration reaches 1.5 for different systems sizes. Diamonds are results for ϕ=0.235 eV and δ=0, and asterisks are results for ϕ=0.235 eV and δ=0.16 eV at 300 K. The dotted line is the prediction of the continuum model with δ=0.

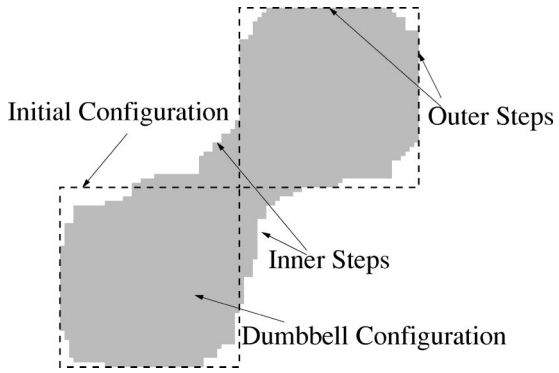

FIG. 9. Illustration of the early stage of dumbbell relaxation. Note the coincidence of the outer layers of the dumbbell configuration with the initial configuration.

for relaxation of convex faceted clusters for the case $\delta=0$, apply to describe behavior for relaxation of rectangular clusters observed in Sec. III B 1. A key conclusion in Refs. 14 and 15 is that crossover behavior (for $\delta=0$) is determined by the relative magnitude of the linear cluster size L and a characteristic length $L_c=\exp[\frac{1}{2}\phi/(k_BT)]$ (≈ 94 lattice constants, for our parameters), which measures the typical separation between kinks on an extended [110] step edge.

Beyond these previous studies, our results reveal that there are two crucial additional factors controlling the relaxation dynamics of 2D nanoclusters and, specifically, the size scaling exponent n: (a) the geometry of the cluster; and (b) the kink rounding barrier δ. Indeed, the $n\approx 3$ behavior for a large δ found in Sec. III A 2 seems to match well previous studies[1] of dumbbell relaxation in the Ag/Ag(100) system at 300 K. Below, we elucidate the dependence of n on these factors in terms of the individual atomistic PD processes. The effective Arrhenius barrier for relaxation is also characterized in terms of the barriers for these individual processes.

For $L \gg L_c$, the step edge is rough due to thermally activated kinks, and the system is well described by the continuum model. The size scaling is given by $n=4$ for all cases, so we provide no detailed discussion of this regime. The following simplified analyses apply to situations where $L \lesssim L_c$.

A. Initial stages of dumbbell evolution: Entropy-driven relaxation

For the initial relaxation of clusters formed by corner-to-corner coalescence, atoms flow primarily from the outer corners towards the inner region, thus developing a neck. At this stage, it is not common to completely remove outer edges of atoms (see Fig. 2 for $\tilde{t}=0.027$). The latter feature implies that this process does not involve a change of energy (as an energy decrease only occurs upon moving the last atom from an outer edge to the neck region).[30]

More explicitly, consider dumbbell configurations of the cluster which retain portions of the four faceted outer edges of the initial configuration (see Fig. 9). Then, provided the four portions of kinked step edges between the faceted regions each have kinks of only one sign, the energy of the dumbbell configuration equals that of the initial configuration. This is most easily seen by noting that (in both cases) the total number of broken bonds equals twice the sum of the distances measuring the span of the cluster along the two major axes. Since there is no change in energy, and since there are clearly many such dumbbell configurations (compared with just one initial configuration), we naturally describe evolution as entropy driven. Although the outer steps are faceted, they do not play an important role in the dynamics. Thus the relaxation process in this regime can be very accurately described by the continuum model. For both the case with $\delta=0$ and $\delta>0$, the size scaling exponent is $n=4$ (cf. Fig. 3 and Fig. 4). The relaxation rate is governed by the PD mobility coefficient $\sigma_{\rm PD}$, with activation energy $E_e+\phi+\delta$.

B. Later stage of dumbbell evolution: Energy-driven relaxation

For the later stage of relaxation of corner-to-corner coalescence, the atoms on the outer steps are removed and attached to the inner steps. When one layer of atoms on the outer steps are completely removed, the cluster can lower its energy. This is similar to the situation in Ref. 15 with one distinction. Here, the inner steps can readily accept atoms from outer steps without first nucleation of a new layer.

At this stage, relaxation is controlled by the removal rate of outer layers of typical size L in the case of $L \lesssim L_c$. The typical time $\tau_{\rm layer}$ for removing a complete layer of L atoms satisfies $\tau_{\rm layer} \sim L^2\tau_0$, where $h_0=\tau_0^{-1}$ is the exchange rate of atoms between two adjacent layers. This result is essentially just Einstein's relation for a system undergoing a random walk between configurations with different numbers of transferred atoms. A more detailed derivation follows from adapting the master equation formalism of Combe and Larralde.[15] In order to relax back to the equilibrium shape $O(L)$ layers have to be removed, so the relaxation time $\tau_{\rm eq}$ scales as $\tau_{\rm eq} \sim L\tau_{\rm layer} \sim L^3\tau_0$.

It thus remains only to develop an appropriate expression for the characteristic time τ_0, for atom exchange between layers in order to obtain an explicit expression for the relaxation time. This is done in Appendix D where we show that $\tau_0 \sim (L_r+L)\tau_k$ (neglecting constants of order unity). Here $(\tau_k)^{-1}=h_k$ is the rate for kink escape, and $L_r=\exp[\delta/(k_BT)]$ is a length scale associated with the extra corner rounding barrier. In our simulations with $\delta=0.16$ eV at 300 K, one has $L_r \approx 490$. L_r is the 1D analog of the so-called Ehrlich-Schwoebel length.[31] If the distance between the kinks is larger than L_r, then the exchange is limited by diffusion of edge atoms. If the distance is smaller than L_r, then it is limited by the rate for corner rounding. Thus we have for $L \lesssim L_c$ that

$$\tau_{\rm eq} \sim \begin{cases} L^4\tau_k & \text{for } L \gg L_r, \\ L^3\tau_c & \text{for } L \ll L_r. \end{cases} \tag{11}$$

The *first case* recovers conventional scaling, $\tau_{\rm eq} \sim L^4$. However, there are some subtleties. The rate is proportional to $h_k=\nu\exp[-(E_e+\phi)/(k_BT)]$. This result follows since here

$L \lesssim L_c$, thus the outer steps are completely faceted. The rate limiting step is the diffusion of a single atom (once it is detached from a kink position) along a faceted step edge, so the rate should scale like h_e times the density of such atoms. In contrast, the continuum model which predicts that the rate is proportional to $h_c = \nu \exp[-(E_e+\phi+\delta)/(k_BT)]$ applies for $L \gg L_c$. The *second case*, $\tau_{eq} \sim L^3$, corresponds to an unconventional scaling law.[32]

C. Evolution of rectangular clusters: Nucleation-limited relaxation

Here, we exploit the ideas developed by Combe and Larralde[15] for relaxation of convex faceted clusters for a generic PD model with no corner rounding barrier on a hexagonal lattice. These ideas can be directly applied to analyze the relaxation of rectangular clusters [created by side-to-side coalescence in metal(100) homoepitaxial systems] for the case $\delta=0$. Furthermore, we also extend this approach to treat $\delta>0$. Specifically, we consider the relaxation of a near-rectangular cluster (dimensions $L \times \lambda L$, with $\lambda>1$) to its near-square equilibrium shape at low T. Again we consider the case of $L \lesssim L_c$ only, so that the edges of the rectangular cluster are faceted. The key process is nucleation and growth of a new terrace on a perfect long edge due to transfer of atoms from the short edge.[15] Successive completion of such new terraces will shift the cluster towards a square shape. However, there is no energetic advantage to nucleation of a new terrace on the long edge (versus the short edge) or to the subsequent mass transfer (and it is quite likely that nucleation occurs on the short edge potentially shifting the shape away from equilibrium). The resolution is this apparent dilemma is that for nucleation on the long edge, subsequent transfer of sufficiently many atoms can completely remove one layer of the short edge. Transfer of the last atom in this process leads to an energy decrease, so the reverse process is very unlikely.[15] In contrast, the latter is not possible for nucleation on the short terrace.

Detailed (but approximate) analysis of the process of complete removal of a layer from the short edge of the clusters can be achieved following Ref. 15. One treats evolution of the system through configurations with various numbers of transferred atoms as a Markov chain, regarding the final configuration as an absorbing or trapping state. Then, one develops and solves an appropriate set of coupled equations for the trapping times starting from various configurations. While this approach yields explicit results including corrections to size scaling, it should be emphasized that these finer details are not so germane to behavior in real systems due to the assumptions in the modeling (e.g., ignoring roughening of the corners of the rectangular cluster, and assuming a perfectly absorbing final state). Thus we prefer here to avoid the complex details of the mathematical analysis, instead focusing on the basic physics which drives the dominant size scaling.

The central result from a mathematical analysis of the above type is that the time for removal of the complete layer has the form $\tau_{layer} \sim L\tau_c/K + L^2\tau_0$, for $L \lesssim L_c$ (neglecting constants of order unity).

The *first* term in τ_{layer} reflects the ''difficult'' nucleation step: after the first atom is ejected from the short edge onto the long edge with low rate h_c, it is much more likely that the system will return to its initial configuration rather than eject a second atom, and nucleate a new layer on the long side. In fact, $K \ll 1$ corresponds to an ''equilibrium constant'' with the following interpretation. Suppose that the system has evolved from the initial perfect rectangular state I to the state S where the first particle has been ejected from the short edge. Let p_- denote the conditional probability that given the system is in S, it returns to I. Let p_+ denote the conditional probability that given the system in S, a second particle is ejected from the short edge and leads to nucleation of a new layer on the long side. Then, one has $p_- + p_+ = 1$, and $K = p_+/p_-$. The *second* term in τ_{layer} reflects the feature that after the new layer is nucleated, the system essentially follows a random walk through configurations with different numbers of atoms transferred between the short and long edges. It is analogous to the Einstein-type relation in Sec. IV B, and $h_0 = \tau_0^{-1}$ is now the exchange rate of atoms between two sides. The analysis in Appendix D shows that $\tau_0 \sim (L_r + L)\tau_k$ has exactly the same form as in Sec. IV B.

Since relaxation back to equilibrium requires transfer of $O(L)$ layers, the relaxation time τ_{eq} has the form

$$\tau_{eq} \sim L\,\tau_{layer} \sim L^2\tau_c/K + L^3\tau_0, \tag{12}$$

for $L \lesssim L_c$. This is our key result for the relaxation time.

The presence of a kink rounding barrier affects both the nucleation process (and specifically the values of τ_c and K), as well as the subsequent mass transfer (as is evident from the explicit form for τ_0). To obtain explicit forms for τ_{eq}, it just remains to determine those for K. For $\delta=0$, the analysis of Ref. 15 shows that $K \sim \exp[-\phi/(k_BT)]$. For large δ, it is clear that if the second atom is ejected from the short edge when the first ejected atom is still on the long edge, then they will almost certainly meet and nucleate a new layer (since the alternative is to return around the corner, which is difficult). Consequently, K is given by the ratio of the rate to eject the second atom h_c to the rate for the first ejected particle to return to the short edge h_r/L (noting that the probability for this atom to be on the corner site is $\sim 1/L$). Thus, finally, one has that $K \sim \exp[-\phi/(k_BT)]L$, for large δ, exceeding the value for $\delta=0$.[33]

For $L \lesssim L_c$, it is easy to check that the first term in Eq. (12) either dominates or comparable to the second term. Thus we can summarize our findings by the relations

$$\tau_{eq} \sim L^2 \exp[\phi/(k_BT)]\tau_k \tag{13}$$

when $\delta=0$, and

$$\tau_{eq} \sim L \exp[\phi/(k_BT)]\tau_c \tag{14}$$

when $\delta>0$ and $L \ll L_r$.

To summarize, in Table I, we list the equilibration time of clusters for different size regimes and geometries.

TABLE I. Characteristic relaxation time for entropy-driven (A), energy driven (B), and nucleation-limited (C) relaxation discussed in Sec. IV. Here τ_c and τ_k stand for the characteristic time for corner breakup and kink escape, respectively, and $\rho = e^{-\phi/(k_B T)}$. Note that the second column applies for $0 \leqslant \delta < \phi/2$. Footnotes indicate which of our MC simulation results illustrate the various regimes.

	$L \ll L_r, L_c$	$L_r \ll L \ll L_c$	$L_c \ll L$
A (entropy)	$L^4 \tau_c$ [a]	$L^4 \tau_c$ [d]	$L^4 \tau_c$
B (energy)	$L^3 \tau_c$ [b]	$L^4 \tau_k$ [b]	$L^4 \tau_c$
C (nucleation)	$L \tau_c \rho^{-1}$ [c]	$L^2 \tau_c \rho^{-1}$ [c]	$L^4 \tau_c$

[a]See Fig. 4.
[b]See Fig. 5.
[c]See Fig. 8.
[d]see Fig. 3.

V. SUMMARY AND CONCLUSION

We have provided a detailed comparison of the predictions of continuum and atomistic models for the sintering of pairs of 2D nanoclusters in metal(100) homoepitaxial systems. For relaxation of dumbbell-shaped clusters formed by corner-to-corner coalescence, the atomistic model *without* an extra corner rounding barrier agrees both qualitatively and quantitatively with the prediction of the continuum model, even for small sizes or low temperatures. However, an extra corner rounding barrier produces a smaller size scaling exponent for the later stage of the sintering process. This result can be utilized to determine from experimental data the basic kinetic properties of step edges, specifically, the existence and magnitude of any kink rounding barrier. Such an analysis indicates the existence of a substantial kink rounding barrier for the Ag/Ag(100) system.[1] For relaxation of rectangular clusters formed by side-to-side coalescence of near square islands, there is a large discrepancy between continuum and atomistic predictions for small sizes or low temperatures. The discrepancy is more extreme in the presence of a corner rounding barrier. All the above types of behavior can be explained in terms of the underlying atomistic PD processes. A particularly relevant recent paper by Pierre-Louis[29] developed a modified continuum theory which can account for the unconventional scaling in the case of faceted clusters.

We have noted in the introduction that several aspects of our analysis extend beyond relaxation of adatom clusters in metal(100) homoepitaxial systems. Clearly in the Mullins regime where $L \gg L_c$ and L_r, the exact continuum theory will apply for advacancy cluster relaxation (with the same anisotropic step edge stiffness and mobility as for adatom clusters). In fact, we have already used such a formulation to successfully describe a novel pinch-off phenomena observed for wormlike advacancy nanoclusters in the Cu/Cu(100) and Ag/Ag(100) systems.[5] However, for smaller L, significant differences in behavior from the corresponding adatom cluster case can emerge due to an expected large asymmetry between activation barriers of single advacancy and single adatom diffusion at step edges. The details of mass flow under PD can be quite different. For vacancy dumbbell restructuring, we do expect an initial entropy driven relaxation, analogous to the adatom case (although the dominant adatom mass flow will be from the neck region outward). Also, scaling should be influenced by the presence of a kink rounding barrier (as with adatom clusters). For the relaxation of rectangular advacancy clusters, details of the kinetics will no doubt be quite different from the nucleation-mediated adatom cluster case. However, energy minimization associated with complete removal of advacancy layers from the short edge of the cluster does presumably drive the process.

ACKNOWLEDGMENTS

This work was supported by NSF Grants EEC-0085604 and CHE-0078596. It was performed at Ames Laboratory, which is operated for the U.S. Department of Energy by Iowa State University under Contract No. W-7405-Eng-82.

APPENDIX A: CLUSTER DIFFUSION VIA PD

For the surface diffusion of large 2D clusters via PD, continuum theory (as well as simple atomistic arguments) predict scaling of diffusion coefficient D with linear size L of the form $D \sim L^{-\alpha}$, with exponent $\alpha = 3$.[34] However, large-scale atomistic simulations of cluster diffusion via PD reveal that α deviates significantly below 3. Furthermore, of particular relevance to this work is the interesting proposal that α is generally related to the exponent n for restructuring via $\alpha = n - 1$.[10,14,35]

Simulations by Mills *et al.* of cluster diffusion at higher T for a generic model for metal(100) homoepitaxy with $\phi = 0.3$ eV recovered $\alpha = 3$ at 800 K, and an activation barrier of $E_{\rm diff} \approx E_c = E_e + \delta + \phi$.[36] However, for lower T, α deviated below 3 (down to 1.2 at 300 K where $L < L_c$), and $E_{\rm diff}$ increased to $\approx E_e + 2\phi$. These authors proposed that diffusion is limited by nucleation of a new edge at a rate of $h_e (n_{\rm eq})^2$, where $n_{\rm eq} \sim \exp[-\phi/(k_B T)]$, implying that $E_{\rm diff} = E_e + 2\phi$. This is just the picture of Jensen *et al.*[14] and of Sec. IV C for relaxation of convex faceted clusters at low T (with $\delta = 0$). Indeed, Jensen *et al.* noted that using $\alpha = n - 1$, their theory also explained the size scaling in Ref. 36.

Experiments also reveal low values of $\alpha \approx 2$ for homoepitaxial metal(100) and metal(111) systems at 300 K where cluster diffusion is known to be controlled by PD.[4,35] It is plausible that this just represents crossover behavior towards nucleation-mediated behavior. Indeed, simulations of our model with $\phi = 0.235$ eV and $\delta = 0$ at 300 K yield $\alpha \approx 1.8$ (cf. $n = 2.7$). One could match the slightly higher experimental values by further decreasing ϕ below 0.235 eV (and by increasing δ well above the value in Ref. 36). As in Sec. III B, the main effect of δ in this temperature range is to decrease the overall step edge atom mobility, and thus the cluster diffusion rate. The effect of δ on the size scaling exponent seems secondary to that of nucleation-limited relaxation which can shift α from 3 to 1.

APPENDIX B: MODEL AND SIMULATION DETAILS

For the most part we follow the so-called Bortz or n-fold algorithm[37] in our kinetic Monte Carlo (KMC) simulations

of the atomistic model with a broad range of hopping rates h_i described in Sec. II A. Surface atoms are categorized into five classes, i.e., with lateral bond number m from 0 to 4. Atoms from each class are chosen with probability proportional to $e^{-m\phi/(k_BT)}$. Once chosen, it can perform either a NN or a second NN (2NN) hopping, with probability proportional to 1 and $e^{-\delta/(k_BT)}$, respectively. The move is accepted provided the site that an atom hop to is vacant. This algorithm is not completely ''reject-free,'' but rather a comprise between efficiency and the programming complexity. We note that in contrast to similar previous studies,[1,14,16] we *do* allow atoms with three or more neighbors to hop. This avoids violating detailed balance, and also avoids the artifact that a close-packed step edge is completely frozen. For the temperature range and relaxation processes considered, behavior of our models is very close to the model where atoms with three NN bonds are immobile.

Finally, we note that disconnected cluster configurations can be generated ''indirectly'' in our model, e.g., if an atom has just one NN which hops away. However, these energy-increasing events are extremely rare, so their effect can be ignored. One can further limit these situations by demanding that atoms must have at least one 2NN after hopping. Such algorithms, which impose some sort of connectivity condition by checking only the state of the hopping atom (and not that of all atoms its neighborhood) are very efficient, but suffer from a weak violation of detailed balance.

APPENDIX C: PD MOBILITY AND ITS MEASUREMENT FROM KMC SIMULATIONS

Following Spohn[38] and Krug *et al.*[13] we define the mobility for periphery diffusion as the linear-response coefficient when an external driving force acts on the step edge atoms in the direction parallel to the step edge, i.e.,

$$\sigma_{\rm PD} = \lim_{F\to 0} J_{\rm PD}(F)/F, \tag{C1}$$

where $F=|\mathbf{F}|$ is the magnitude of the external driving force, and $J_{\rm PD}(F)$ is the magnitude of the net flux. The external driving force produces biases in the hopping rates. In our algorithm we assign different probabilities for choosing various hopping directions,[13] e.g.,

$$p(x\to x+a, y\to y) \sim (1+f_x a/2),$$
$$p(x\to x+a, y\to y+a) \sim (1+f_x a/2+f_y a/2), \tag{C2}$$

to linear order in F. We then measure the net flux $J=(J_x+J_y)^{1/2}$ directly from Monte Carlo (MC) simulation using this bias. Figure 10 shows the θ dependence of the mobility (in unit of ah_e) for various δ values. We can see that for $\delta=0$, $\sigma_{\rm PD}$ is almost isotropic (within 6%), with $\sigma_{\rm PD}$ given approximately by $ah_e e^{-\phi/(k_BT)}$. As δ increases, anisotropy increases and the overall mobility decreases.

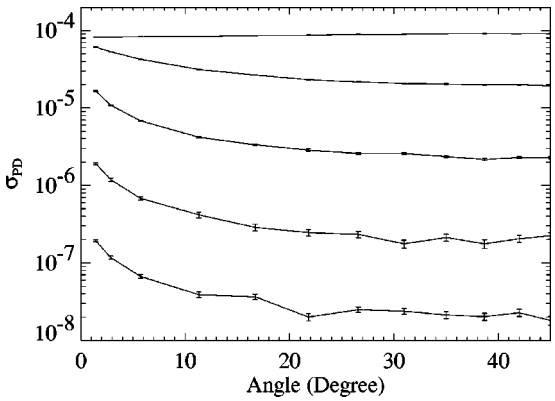

FIG. 10. Angular dependence of the atom mobility for periphery diffusion measured from Monte Carlo simulations with $\phi = 9.4k_BT$. From top to bottom, one has $\delta/\phi=0$, 1/4, 1/2, 3/4, and 1. The mobility is measured in unit of $h_e a$, where h_e is the edge diffusion rate. The same attempt frequency is used for both NN and second NN hopping.

APPENDIX D: CORNER ROUNDING PROBABILITIES AND TIME SCALES

We analyze a process involving atom detachment from a kink site, diffusion along L_1 sites on a [110] step edge, rounding of a corner, diffusion along L_2 sites on a [110] step edge, and attachment to another kink; see Fig. 11(a). Thus we label the linear array of sites traversed by $j=1$ to L_1+L_2, bounded by traps at $j=0$ and L_1+L_2+1. Hopping occurs randomly between adjacent sites at rate h_e, except between sites L_1 and L_1+1 at rate h_r, and there is no escape from traps. Below we set $p=h_r/(h_e+h_r)$, $q=h_e/(h_e+h_r)=1-p$, and $L_r=h_e/h_r=\exp[\delta/(k_BT)]$. Let P_j denote the probability that an atom starting on site j is trapped at site

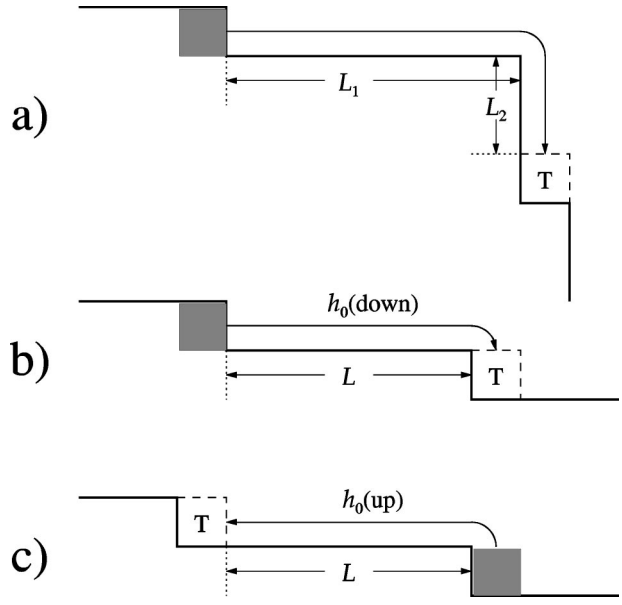

FIG. 11. Transfer of atoms (shaded squares) around corners to traps at kink sites (denoted by T). Distances are in units of the lattice constant a.

L_1+L_2+1, so $P_0=0$ and $P_{L_1+L_2+1}=1$. Then, one has that

$$P_j=1/2(P_{j-1}+P_{j+1}), \tag{D1}$$

where $1\leqslant j<L_1$ and $L_1+1<j\leqslant L_1+L_2$, and

$$P_{L_1}=qP_{L_1-1}+pP_{L_1+1},$$
$$P_{L_1+1}=pP_{L_1}+qP_{L_1+2}, \tag{D2}$$

where Eq. (D2) accounts for the reduced hop rate to round corners. From the first relation, the solution is piecewise-linear in j, i.e., $P_j=Aj$ for $j\leqslant L_1$, and $P_j=1-B(L_1+L_2+1-j)$ for $j\geqslant L_1+1$. The latter relations determine $A=B=h_r/[h_e+h_r(L_1+L_2)]$, so that $P_1=1/(L_r+L_1+L_2)$.

For atom transfer between faceted edges, discussed in Sec. IV C, the characteristic rate is $h_0\approx h_kP_1$ (the product of the microscopic kink detachment rate, and the probability to successfully round the corner), where here we set $L_1+L_2=L$. Thus one obtains $\tau_0=h_0^{-1}\approx(L_r+L)\tau_k$. For atom transfer between layers discussed in Sec. IV B, one has characteristic rates of $h_0(\text{down})\approx h_kP_1(L_1=L,L_2=0)$ for downward transport [Fig. 11(b)], and $h_0(\text{up})\approx h_cP_1(L_1=0,L_2=L)$ for upward transport [Fig. 11(c)], which in both cases recovers $\tau_0=h_0^{-1}\approx(L_r+L)\tau_k$.

Finally, we note that one can develop and solve a coupled set of equations for the trapping times t_j for a particle starting from various sites j (cf. Ref. 15). Here, we assume that if the particle returns to the initial kink site, then it can escape from that site again at rate h_k, and thus finally reach the destination trap site. The results of this analysis recover those above using an approach based on corner rounding probabilities, and also produce small correction terms (e.g., an additional term scaling like $L^2\tau_e$ for $\delta=0$).

[1] C. R. Stoldt, A. M. Cadilhe, C. J. Jenks, J.-M. Wen, J. W. Evans, and P. A. Thiel, Phys. Rev. Lett. **81**, 2950 (1998); C. R. Stoldt, A. M. Cadilhe, M. C. Bartelt, C. J. Jenks, P. A. Thiel, and J. W. Evans, Prog. Surf. Sci. **59**, 67 (1998); P. A. Thiel and J. W. Evans, J. Phys. Chem. B **104**, 1663 (2000).

[2] J. F. Wendelken, A. K. Swan, W. W. Pai, and J.-K. Zuo, in *Morphological Organization in Epitaxial Growth and Removal*, edited by Z. Zhang and M. G. Lagally (World Scientific, Singapore, 1998), p. 320.

[3] J. Eggers, Phys. Rev. Lett. **80**, 2634 (1998).

[4] W. W. Pai, A. K. Swan, Z. Zhang, and J. F. Wendelken, Phys. Rev. Lett. **79**, 3210 (1997).

[5] W. W. Pai, J. F. Wendelken, C. R. Stoldt, P. A. Thiel, J. W. Evans, and D.-J. Liu, Phys. Rev. Lett. **86**, 3088 (2001).

[6] J. Heinonen, I. Koponen, J. Merikoski, and T. Ala-Nissila, Phys. Rev. Lett. **82**, 2733 (1999) propose that terrace diffusion of advacancies (TDV) could dominate mass transport in these systems. This claim was based on simulations with $E_v=E_e$, but we expect that E_v significantly exceeds E_e, which favors PD. See Sec. II.

[7] C. Herring, Phys. Rev. **82**, 87 (1951); W. W. Mullins, J. Appl. Phys. **28**, 333 (1957); **30**, 1826 (1959); F. A. Nicholis and W. W. Mullins, *ibid.* **36**, 1826 (1965).

[8] N. C. Bartelt, J. L. Goldberg, T. L. Einstein, and E. D. Williams, Surf. Sci. **273**, 252 (1992).

[9] M. S. Hoogeman, M. A. J. Klik, R. van Gastel, and J. W. M. Frenken, J. Phys.: Condens. Matter **11**, 4349 (1999).

[10] M. Eßer, K. Morgenstern, G. Rosenfeld, and G. Comsa, Surf. Sci. **402-404**, 341 (1998).

[11] M. Giesen and G. Schulze Icking-Konert, Surf. Sci. **412/413**, 645 (1998).

[12] W. Selke and P. M. Duxbury, Phys. Rev. B **52**, 17 468 (1995).

[13] J. Krug, H. T. Dobbs, and S. Majaniemi, Z. Phys. B: Condens. Matter **97**, 281 (1995).

[14] P. Jensen, N. Combe, H. Larralde, J. L. Barrat, C. Misbah, and A. Pimpinelli, Eur. Phys. J. B **11**, 497 (1999).

[15] N. Combe and H. Larralde, Phys. Rev. B **62**, 16 074 (2000).

[16] S. Liu and H. Metiu, Surf. Sci. **405**, L497 (1998); H. Shao, S. Liu, and H. Metiu, Phys. Rev. B **51**, 7827 (1995).

[17] O. Pierre-Louis, M. R. D'Orsogna, and T. L. Einstein, Phys. Rev. Lett. **82**, 3661 (1999).

[18] A. M. Cadilhe, C. R. Stoldt, C. J. Jenks, P. A. Thiel, and J. W. Evans, Phys. Rev. B **61**, 4910 (2000).

[19] A. F. Voter, Proc. SPIE **821**, 6819 (1987); H. Mehl, O. Biham, I. Furman, and M. Karimi, Phys. Rev. B **60**, 2106 (1999).

[20] C.-M. Zhang, M. C. Bartelt, J.-M. Wen, C. J. Jenks, J. W. Evans, and P. A. Thiel, Surf. Sci. **406**, 178 (1998); L. Bardotti, C. R. Stoldt, C. J. Jenks, M. C. Bartelt, J. W. Evans, and P. A. Thiel, Phys. Rev. B **57**, 12 544 (1998). See also Ref. 1.

[21] B. D. Yu and M. Scheffler, Phys. Rev. B **55**, 13 916 (1997).

[22] I. Furman, O. Biham, J.-K. Zuo, A. K. Swan, and J. F. Wendelken, Phys. Rev. B **62**, R10 649 (2000).

[23] G. Boisvert and L. J. Lewis, Phys. Rev. B **56**, 7643 (1997).

[24] U. Kürpick and T. S. Rahman, Phys. Rev. B **57**, 2482 (1998).

[25] C. Rottman and M. Wortis, Phys. Rev. B **24**, 6274 (1981).

[26] R. K. P. Zia, J. Stat. Phys. **45**, 801 (1986).

[27] J. A. Sethian, *Level Set Methods: Evolving Interfaces in Geometry, Fluid Mechanics, Computer Vison, and Material Science* (Cambridge University Press, Cambridge, England, 1996).

[28] W. E. Schiesser, *The Numerical Method of Lines: Integration of Partial Differential Equations* (Academic Press, San Diego, 1991).

[29] O. Pierre-Louis, Phys. Rev. Lett. **87**, 106104 (2001).

[30] There may be an initial increase in energy (aside from fluctuations), especially for larger clusters. This would be associated with formation of additional outer layers during rounding of corners.

[31] P. Politi and J. Villain, Phys. Rev. B **54**, 5114 (1996).

[32] A. M. Cadilhe (unpublished) proposed a similar random-walk-type analysis for decay of bumps at step edges (Ref. 1) for large δ.

[33] The presence of a corner rounding barrier facilitates nucleation of a new layer once the first atom is ejected, however, it slows down the overall process due to the extra factor of $\exp[\delta/(k_BT)]$ in τ_c which appears in Eq. (12).

[34] S. V. Khare, N. C. Bartelt, and T. L. Einstein, Phys. Rev. Lett. **75**, 2148 (1995).
[35] G. Rosenfeld, K. Morgenstern, and G. Comsa, in *Surface Diffusion: Atomistic and Collective Processes*, edited by M. C. Tringides (Plenum Press, New York, 1997).
[36] G. Mills, T. R. Mattsson, L. Møllnitz, and H. Metiu, J. Chem. Phys. **111**, 8639 (1999).
[37] A. B. Bortz, M. H. Kalos, and J. L. Lebowitz, J. Comput. Phys. **17**, 10 (1975).
[38] H. Spohn, J. Stat. Phys. **71**, 1081 (1993).